16TH EUROPEAN CONFERENCE ON EARTHQUAKE ENGINEERING THESSALONIKI 18 - 21 JUNE 2018

EFFECT OF DAMPING MODELS ON THE SIMULATION OF SEISMIC AXIAL FORCES IN A REINFORCED CONCRETE BRIDGE PIER

João P. ALMEIDA[1], Manuel JORDAN[2], Katrin BEYER[3]

ABSTRACT

Post-reconnaissance findings after recent earthquakes have shown that the effect of the vertical acceleration component of the ground motion can be more damaging than typically considered thus far, particularly in near-field regions where the ratio of vertical-to-horizontal ground accelerations may exceed considerably the 2/3 scaling factor used in design. Besides, the usual period range for the constant-acceleration region of vertical acceleration spectra often overlaps with the range of vertical vibration periods in reinforced concrete (RC) structures. These reasons explain the appearance of large dynamic axial forces, which can reduce the column shear strength due to tensile demands or alternatively promote direct compressive failures. Estimating the change in the member axial forces during nonlinear seismic response due to the vertical ground motion component is therefore of paramount significance and can only be simulated through dynamic analyses, for which a specific damping model needs to be assigned. Using a cantilever bridge pier with a top mass as an illustrative example, the present paper assesses the effects of the most commonly used damping models and damping values on the simulation of axial forces. Distributed plasticity beam elements with distinct formulations are employed, and a range of top masses is considered. The results show that, even for very low damping values, distinct damping models can have a very significant influence on the simulation of the seismically-induced axial forces, which increases considerably for larger values of the top mass.

Keywords: Reinforced concrete; Damping models; Axial forces; Vertical acceleration; Beam elements

1. INTRODUCTION

Many design codes suggest the consideration of the effects of the vertical ground motion for specific cases (e.g., long-span horizontal structural members or cantilevers, beams supporting columns) by the application of a vertical spectrum directly scaled from the horizontal one. This procedure was originally proposed by Newmark et al. (1973). A scaling factor of around 2/3 is generally indicated, which was thought to be in general the maximum ratio between vertical and horizontal accelerations in most ground movements (Newmark and Hall 1982). However, aside from those specific cases, in common engineering practice the effect of the vertical ground motion is usually neglected in design and assessment of reinforced concrete (RC) structures. The assumed justification is that gravity-design considerations provide a high factor of safety in the vertical direction, and that additionally the vertical and horizontal ground motions may be significantly out-of-phase.

However, over the past two decades this approach was shown to be unrealistic. Firstly, as discussed below, the vertical-to-horizontal ratio of acceleration (V/H) highly depends on the spectral period. Secondly, the use of a 2/3 factor can be highly non-conservative for near-fault ground motions (while it can be over-conservative for far-fault regions). Studies wherein the typical features of vertical and horizontal components of near-field ground motions were considered showed that the vertical ground

[1]Research Associate, Earthquake Engineering and Structural Dynamics, École Polytechnique Fédérale de Lausanne, Lausanne, Switzerland, joao.almeida@epfl.ch

[2]Former EPFL Master student, now: Design Engineer, Kissling+Zbinden AG, Thun, Switzerland, manuel.jordan@kzag.ch

[3]Associate Professor, Earthquake Engineering and Structural Dynamics, École Polytechnique Fédérale de Lausanne, Switzerland, katrin.beyer@epfl.ch

motion can significantly affect the axial force demand in RC columns both in tension and compression. Additionally, shear failure may be of concern as demand exceeds supply (Papazoglou and Elnashai 1996). This is true namely when tension forces occur, typically for low to intermediate levels of axial load ratio, for which brittle failure mechanisms associated to the reduction of the shear capacity may show up (Di Sarno et al. 2011). The unfavourable influence of the axial force variation due to the vertical component of the ground motion on the shear capacity of RC bridge piers was also confirmed in other investigations (Kim et al. 2011a, 2011b; Lee and Mosalam 2014).

The findings above, combined with the observation of the effects of vertical acceleration after past earthquakes, indicate that estimating the dynamic axial forces arising from vertical ground motion components can be of particular relevance in many cases. The only type of numerical analyses with vertical component allowing for a realistic simulation of the axial force demands are the so-called nonlinear dynamic procedures. They were used for instance by Di Sarno et al. (2011), after the 2009 L'Aquila earthquake, to show that the vertical component increases the shear demand and reduces the shear capacity of RC columns due to large variations of the axial forces.

Past studies investigating the effect of the mass vertical acceleration (with or without consideration of the vertical component of the ground motion) on the structural response focussed mainly on the comparison between experimental and numerical results. However, the influence of different modelling approaches on the results was not consistently analysed. In particular, as far as the authors are aware, no study on the influence of damping models and damping values on the simulation of the axial forces in RC structures has been carried out. That is the main purpose of the present paper.

2. NEAR-FIELD GROUND MOTIONS AND EFFECTS OF VERTICAL ACCELERATION

2.1 Characteristics of Near-field Ground Motions

The relevance of near-fault effects in structures has re-emerged in the past years following new compelling field evidence collected after recent earthquakes, namely L'Aquila in 2009 and Christchurch in 2011. A near-field zone is typically considered within 15 km (Ambraseys and Simpson 1996) to 20 km (Bray and Rodriguez-Marek 2004) from the fault rupture. This is the case of the 2011 *Christchurch* ground motions CHHC and PRPC – see Table 1, recorded at epicentral distances of 8 and 6 km respectively, which are used later in this study. The original acceleration-, velocity- and displacement-time series were obtained from GeoNet (2016). Near-field records are characterized by a few long-period, large-amplitude, and short-duration velocity pulses.

Studies from the mid 90's (Bozorgnia and Niazi 1993; Bozorgnia et al. 1995) have shown that the V/H ratio is very sensitive to the spectral period, site-to-source distance, and earthquake magnitude. Later, it was found that local site conditions also strongly influence the V/H spectra, while they are a relatively weak function of earthquake magnitude and faulting mechanism (Bozorgnia and Campbell 2004). For short periods, the near-field V/H spectral ratio is larger than for the far-field, and largely exceeds the commonly assumed ratio of 2/3. Well-known earthquakes where the vertical component of the ground motion was relevant include the 1979 Imperial Valley, 1994 Northridge, 1995 Hyogo Ken Nanbu (Kobe), 1999 Chi-chi, 2009 L'Aquila, and 2011 Christchurch, which showed $(PGA)_v/(PGA)_h$ ratios of 2.68, 1.79, 1.63, 1.13, 1.16 and 2.45 respectively. On the other hand, the V/H spectral ratio reduces to less than 2/3 at long periods. These characteristics are illustrated in Figure 1, which shows the elastic response spectra of the two horizontal and the vertical component of the CHHC ground motion record.

It is noted that the time interval between the occurrence of the peak ground acceleration (PGA) of the horizontal and vertical components increases as the distance source-to-site increases. The horizontal and vertical ground motion peaks can be coincident for distances less than 5 km and such time lag is generally less than 5 s for distances below 25 km (Collier and Elnashai 2001).

Table 1. Characteristics of the M_w 6.2 Christchurch 2011 near-field ground motions used in the present study.

Record		D	Direction /	$(PGA)_h$	$(PGA)_v$	$(PGA)_v$ / $(PGA)_h$	Scaling factor
Designation	**Acronym**	**[km]**	**Component**	**[g]**	**[g]**	**[-]**	**[-]**
Christchurch Hospital	CHHC	8	S89W	0.36	0.51	1.42	1
Pages Road Pumping Station	PRPC	6	W	0.66	1.63	2.45	0.54

Legend: D - Epicentral distance; $(PGA)_h$ - Peak ground acceleration in the horizontal direction; $(PGA)_v$ - Peak ground acceleration in the vertical direction; Scaling factor - scaling factor applied to the ground motion to run the numerical simulations.

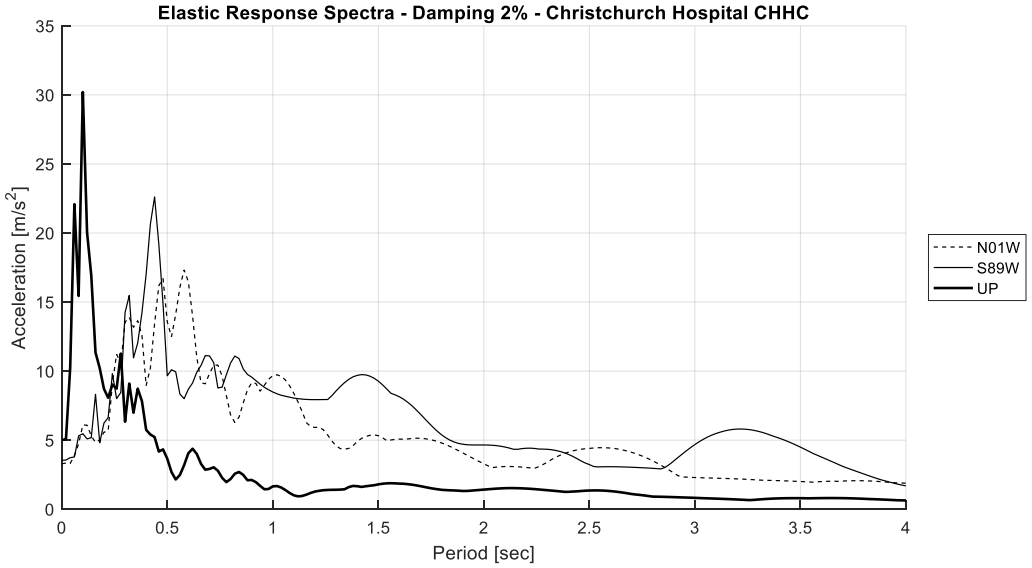

Figure 1. 2011 Christchurch ground motion CHHC: Elastic acceleration response spectra for 2% damping, for both horizontal components N-W and S-W, and the vertical component (GeoNet 2016).

2.2 Effects of Vertical Acceleration

Many earthquakes in the past revealed the non-negligible effect of the vertical acceleration on the structural response, above all on the axial force variation in vertical load bearing elements. Papazoglou and Elnashai (1996) presented field evidence on the effects of strong vertical ground motion on buildings and bridges, taken from post-earthquake reconnaissance missions after the 1986 Kalamata (Greece) earthquake, the 1994 Northridge (California) earthquake, and the 1995 Hyogo Ken Nanbu (Japan) earthquake. Several failures of RC and masonry structures during the 2009 L'Aquila (Italy) earthquake, as well as of non-structural components supported by cantilever systems, have also been attributed to the effects of the vertical seismic action (Di Sarno et al. 2011). The collapse of many unreinforced masonry buildings close to the epicentre of the 2011 New Zealand Christchurch earthquake also seems to have been the result of the strong velocity pulses and the large vertical ground accelerations (Cooper et al. 2012).

Unlike horizontal periods, vertical periods of a wide range of RC buildings and bridges typically fall within a relatively narrow interval of around 0.025-0.25 sec. Considering that the constant acceleration range for the vertical ground-motion lies between 0.05-0.15 sec (see also Figure 1), it can be expected that large dynamic axial forces show up. They can lead columns into direct tension (usually in the upper storeys), with consequent reduction of shear strength and ductility supply, or to fail in a brittle mode by direct compressive failure (usually in the bottom storeys). It is also argued that interior columns of RC frames are more vulnerable to the effects of vertical ground motion as their design is less influenced by increased axial loads due to overturning moment, and that failure of capacity-designed columns is more likely to occur at mid-height of internal columns at upper storeys, outside the well-detailed plastic hinge regions of the member (Papazoglou and Elnashai 1996).

3. SHORT REVIEW ON DAMPING MODELS FOR NUMERICAL SIMULATION

Within the scope of nonlinear frame modelling adopted in the current study, the majority of the dissipated energy is explicitly accounted for through hysteretic material models. The use of generalized damping is however needed to reproduce sources of energy dissipation that, given their phenomenological complexity, are difficult to be simulated explicitly. Hence, the required damping for a given nonlinear dynamic analysis will necessarily depend on the level of detail of the finite element model assembled. In view of the difficulties to identify and mathematically describe each of the dissipating mechanisms in actual structures, damping is usually represented in a highly idealized manner by a set of generalized linear viscous dampers. The damping coefficients are defined such that the dissipated energy is approximately equivalent to the energy associated to all non-modelled dissipation mechanisms. This idealisation, first introduced by Jacobsen (1930), is therefore called equivalent viscous damping. For the overwhelming majority of structural engineering software, the latter takes on the form of Rayleigh damping (RD), which combines stiffness- and mass-proportional components. Its computational attractiveness comes from the fact that it does not require the computation of new matrices, while keeping the sparsity of the stiffness matrix (Chopra and Mckenna 2017). The main problems of this approach are briefly summarised below.

First off, stiffness-proportional damping (SPD), regardless of being initial stiffness-proportional damping (ISPD) or tangent stiffness-proportional damping (TSPD), may introduce artificial and significantly large axial forces in the members, leading to convergence issues and potential instability during the analyses. Moreover, as demonstrated by Correia et al. (2013), when stiffness-proportional damping is employed the member forces are not in equilibrium with the support reactions.

According to ISPD, damping forces remain proportional to their elastic stiffness regardless of the ductility demand. Hence, this solution may result in an overestimation of the energy dissipated through viscous damping. Analyses performed by Priestley and Grant (2005) indicate that the energy absorbed by elastic damping in ISPD may approximate the energy dissipated through hysteresis, even for large ductility levels. Consequently, it is very likely that such damping model produces a significant underestimation of peak response displacements during nonlinear dynamic analyses. Moreover, as in general the structural stiffness decreases during earthquake loading, the damping forces may assume unrealistically large values when compared to the member (restoring) forces (Hall 2006). Furthermore, Bernal (1994) showed that spurious damping forces are likely to arise in massless degrees of freedom (or with relatively small inertia); the latter tend to undergo abrupt variations in velocity when stiffness changes, leading to unrealistically large viscous damping forces (Jehel et al. 2014).

TSPD appears clearly preferable to ISPD (Grant et al. 2005) since it: (i) significantly reduces spurious damping forces (Charney 2008), and (ii) models a decrease in the dissipated energy for increasing ductility demands, which can be considered as intuitively meaningful. On the other hand, Chopra and McKenna (2017) criticise its physical and conceptual basis, arguing that sudden drops in damping force when yielding occurs, and triangular loops in force-velocity relations, are unacceptable. Moreover, when the stiffness matrix becomes negative-definite, TSPD leads to an unrealistic energy input in the structure.

Mass-proportional damping, despite not having a physically justifiable support, does not exhibit the numerical deficiencies of the previous models. Nonetheless, Hall (2006) reported several weaknesses when large rigid-body modes occur, leading to excessively high velocities; such situation is not common in typical structures but may be important, e.g., when dealing with base isolated buildings. In addition, the damping ratio in MPD models decreases exponentially with a decrease of the vibration period, thus possibly leading to an underdamped higher-mode response.

Recently, several studies addressed some of the abovementioned limitations of Rayleigh damping. They defend the application of existing alternatives, such as superposition of modal damping matrices (Chopra and McKenna 2016), or propose new models (Puthanpurayil et al. 2016; Lanzi and Luco 2017). However, the present study restricts to the use of RD as it is the only model widely implemented in analysis software and available for engineering practice.

4. CASE-STUDY

4.1 Description of Structure and Nonlinear Model

The structure analysed in this study is based on a cantilevered bridge pier that was tested on the *NEES Large High-Performance Outdoor Shake Table* at UCSD's *Englekirk Structural Engineering Center* under a wide range of ground motions (Terzic et al. 2015). This circular column, whose design is consistent with the current Caltrans design practice (Department of Transportation of California), is 7.32 m high, has a diameter of 1.22 m, and a concrete cover thickness of 67 mm. Details on the reinforcement layout and geometry can be found in Figure 2.

The actual reinforced concrete block on the top of the bridge pier had a mass of 228 ton, which corresponds to an axial load ratio of around 4%. However, for the current investigation, analyses were conducted with a range of lumped masses varying from 0 to 1500 ton, which produce an axial load ratio between 0% and 25%. The mass was also obviously assigned to the vertical direction. The previous interval covers the usual range of horizontal and vertical periods for RC structures (Papazoglou and Elnashai 1996). For simplicity, no rotational inertia was considered, as assumed in other studies (Di Sarno et al. 2011). The Hilber-Hughes-Taylor method was employed as the numerical time-domain integration scheme (Hilber et al. 1977).

The column is modelled with distributed plasticity Euler-Bernoulli beam elements. It was decided to investigate both force-based (FB) and displacement-based (DB) beam formulations since it is well known that the latter verifies equilibrium on an average sense, which has serious consequences on the distribution of axial forces among the element integration points (IPs) (Calabrese et al. 2010). Consequently, the two following meshes were used to model the bridge pier:

- One FB element with five Gauss-Lobatto IPs.
- Four DB elements with two IPs each. The bottom element length was defined as roughly 1.65 m, estimated according to the plastic hinge length formula by Priestley et al. (2007); the remaining three elements were assigned equal lengths.

Geometric nonlinearity is taken into account with a corotational formulation, which models the effects of large nodal displacements. Material nonlinearity at the sectional level is considered by 300 axially-behaving fibres, whose constitutive response is governed by the models described below.

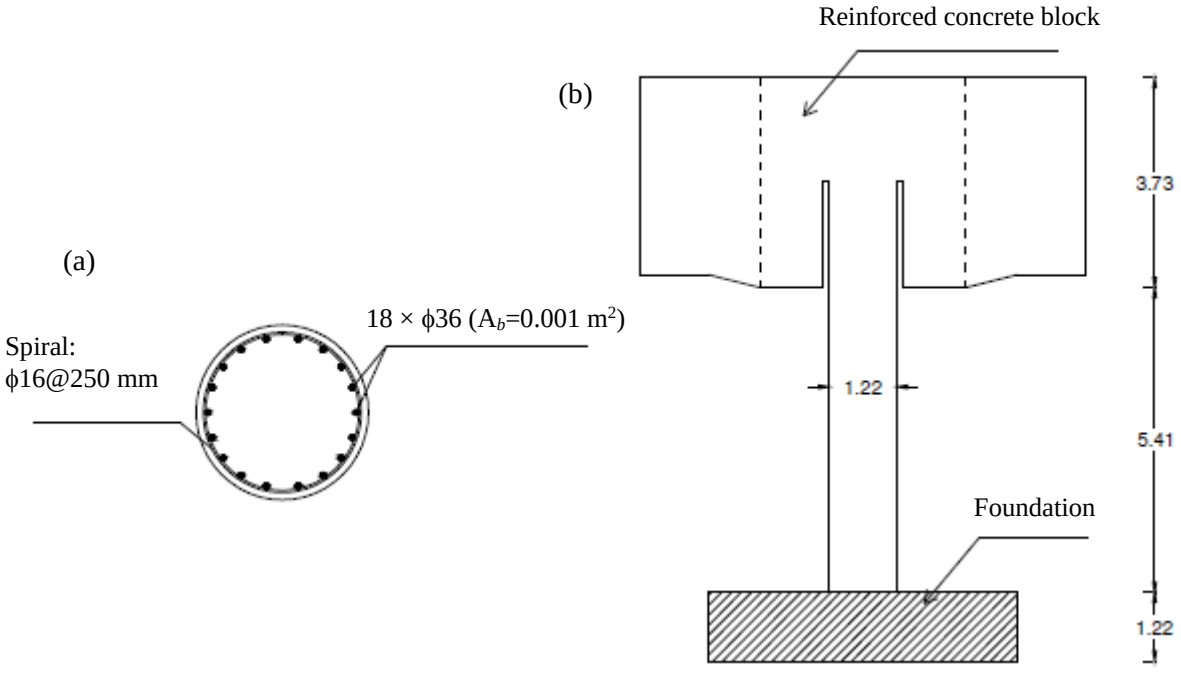

Figure 2. (a) Bridge column cross-section. (b) Geometrical dimensions of the column [m] (Terzic et al. 2015).

Table 2. Lateral and vertical periods for four illustrative values of the top mass.

Lumped mass	Axial load ratio	Period	
		Horizontal (X)	Vertical (Z)
[ton]	[%]	[sec]	[sec]
0	0	0.117	0.009
500	8.6	0.813	0.060
1000	17.1	1.144	0.084
1500	25.7	1.400	0.103

The model by Mander et al. (1988) was used for the concrete, with the following parameters: compressive strength of 41.5 MPa, modulus of elasticity of 32.2 GPa, and strain at peak stress of 0.0028. Tensile strength was neglected. A confinement factor of 1.2 was assigned to the core fibres. The steel rebars were modelled by the Menegotto-Pinto model (Menegotto and Pinto 1973) with the isotropic hardening rules proposed by Filippou, Popov, and Bertero (1983). The material parameters are: yield strength of 518.5 MPa, modulus of elasticity of 200 GPa, strain hardening parameter of 0.008, fracture strain of 0.1, transition curve initial parameter of 20, A1 = 18.5, A2 = 0.15, A3=0, and A4 = 1.

The three rotations and translations at the column base node were blocked, while no restraints were defined at the bridge top. The applied ground motions are indicated in Table 1, which also depicts the scaling factor of the horizontal and vertical components of the PRPC record. The resulting scaled $(PGA)_{h,PRPC}$ is equal to the $(PGA)_{h,CHHC}$ =0.36g. Planar analyses are performed; the horizontal component displaying larger velocity pulses in the velocity-time history is chosen to be applied to the pier base. The model and nonlinear dynamic analyses were performed with the software *SeismoStruct* (SeismoSoft 2016) and double checked with *OpenSees* (OpenSees 2013). Axial forces (positive for compression, negative for tension) were extracted at the support. Table 2 shows the fundamental periods obtained in the horizontal (X) and vertical (Z) directions for four illustrative cases of different lumped masses at the top of the bridge pier.

4.2 Sensitivity Study

The following damping models, which as discussed in Section 3 intend to take into account the non-modelled sources of energy dissipation, were analysed for the range of lumped masses and element formulations described in the previous section:

- Tangent stiffness-proportional damping (TSPD) with damping ratio assigned to the horizontal vibration frequency. Commonly, engineers use Rayleigh damping with damping ratios that are assigned to the natural frequencies of the modes that mostly contribute to the lateral response of the structure. It is therefore rare that the damping ratio corresponding to the higher frequency is defined for a vertical vibration mode. In other words, the results obtained with the TSPD model applied to this idealized bridge pier should be also representative of the results expected from the conventional application of Rayleigh damping (with tangent-stiffness proportional component) to a RC frame building or bridge.
- Mass-proportional damping (MPD), again with damping ratio assigned to the lateral vibration frequency.
- Rayleigh damping (RD) with the same damping ratio assigned to the horizontal and vertical vibration frequencies. Empirical evidence does not support the use of different values of damping ratios for the horizontal and vertical vibration modes (as in the two previous options, TSPD and MPD). The stiffness matrix for this RD is assumed to be the tangent-stiffness.
- No damping.

Low values of damping ratio (1%, 2%, and 3%) were defined for the periods described in the approaches above. This is accordance with literature recommendations (Correia et al. 2013). Finally, in some analyses only the horizontal component of the ground motion was applied (X), while in others the horizontal and vertical components were both activated (X+Z).

5. INFLUENCE OF DAMPING MODELS

5.1 Lateral Drift

The influence of the damping models described in the previous section is shown in Figure 3 regarding the maximum lateral pier drift, for the CHHC ground motion record when one FB element is used. Convergence could not be achieved for all analysis cases. It can be seen that, despite the small variation of the damping values, the response scatter increases and is significant for larger values of the top mass (i.e., for larger periods and axial load ratios). The upper-bound estimates are 30% and 57% larger than the lower-bound estimates for lumped masses of 300 ton and 700 ton respectively (equivalent to axial load ratios of 5% and 12%). Additionally, the analyses where the vertical ground motion component was applied (X+Z) consistently provided larger values of the maximum drift in comparison with the cases where only the horizontal component was considered (X). However, this latter effect does not appear to be significant.

5.2 Axial Forces

The influence of damping models can be addressed not only with respect to the maximum lateral drift, but also with regards to other engineering demand parameters, such as axial force, base shear, or base moment. Due to space limitations and as previously discussed, the present study focus on the axial forces. To start with, it should be noted that different effects contribute to the variation of the axial force around its gravity-induced value: (i) As the bottom region of the pier enters the nonlinear range, a shift of the neutral axis occurs at the base IP(s) (i.e., average axial strain increases) and the consequent elongation of the column excites the vertical vibration mode, (ii) If the vertical component of the ground motion is applied, it will directly excite the vertical vibration mode, (iii) The equivalent viscous damping model will induce axial forces since the vertical degree-of-freedom undergoes time-history velocity response; this effect depends on the type of damping model and values, and (iv) The weak-form verification of axial equilibrium if DB elements are used, as noted in Section 4.1. Effects (i) and (ii) only occur when a vertical mass (and vertical vibration mode) is accounted for in the model, while effects (iii) and (iv) will occur even without vertical mass.

5.2.1 Maximum Compressive Forces

Figure 4 and Figure 5 below show the maximum compressive forces attained during the CHHC and scaled PRPC ground motions respectively, using one FB element. Figure 6 plots the results for the latter record using a four-element DB mesh. The following conclusions can be drawn:

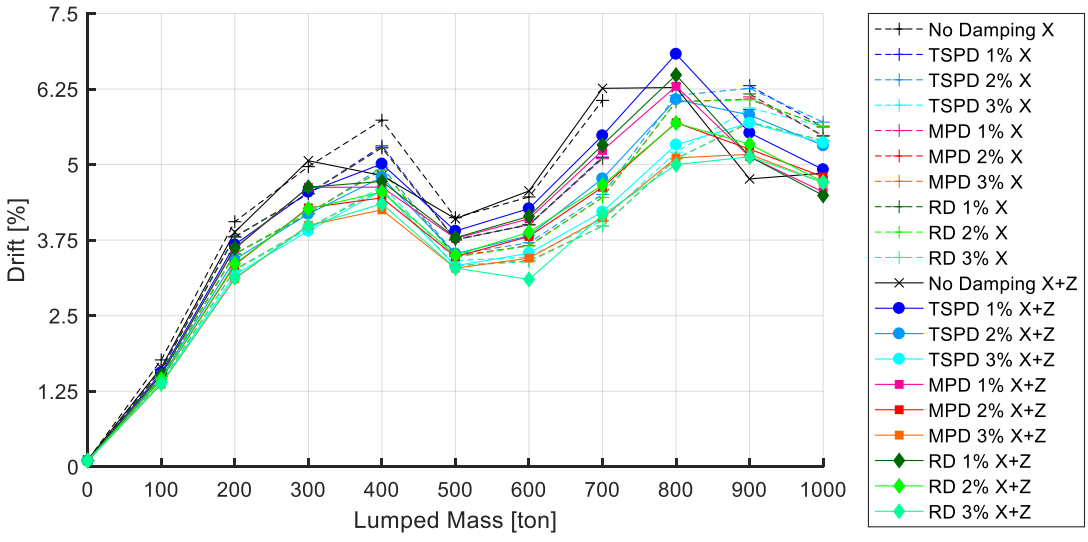

Figure 3. Maximum lateral drift for CHHC ground motion, using one FB element.

- Three main groups of curves can be identified (herein called bottom, middle, and top groups).
- The results obtained with the bottom group, i.e. when only the horizontal ground motion was applied (X), show that the maximum axial force closely follows the applied gravity load. The influence of the damping models and values is minor. This further indicates that the effect (i) described above does not appear to play an important role in this case, suggesting that the level of nonlinearity at the column base is limited.
- On the other hand, the influence of the vertical component of the ground motion (X+Z) is largely apparent from the responses of the middle and top groups. The maximum compressive force in the column can be several times larger than when the horizontal ground motion component alone is considered. Effect (ii) described above is therefore extremely significant.
- The results of the top group correspond to the application of RD, MPD, and no damping. For MPD, the damping ratio of the vertical mode is extremely low (below 0.22%, therefore negligible) and thus the effects of the vertical ground motion can be straightforwardly observed. Unsurprisingly, the results without damping are mingled with the latter. For Rayleigh damping, the damping ratio for the vertical mode is slightly larger (1%, 2%, or 3%), which explains why the corresponding curves are generally below those for MPD.
- The results of the middle group correspond to the application of TSPD (with horizontal and vertical ground motion components, X+Z). The corresponding maximum compressive forces are reduced with respect to the top group, explained by the much increased damping ratio of the vertical mode. Additionally, it can be observed that small changes in the assigned damping values (from 1% to 3%) can produce differences between maximum compressive forces of up to 36%.
- The previous points illustrate the relevance of effect (iii) and how it shows up.
- The values of the compressive forces (middle and top groups) for the PRPC record are significantly larger than for the CHHC ground motion, which further reinforces the fundamental effect of the vertical ground motion component: it is recalled that the ratio $(PGA)_v/(PGA)_h$ increases from 1.42 (CHHC) to 2.45 (PRPC), see Table 1.
- The maximum compressive forces obtained with the DB mesh (Figure 6) are generally consistent with the results obtained with the FB formulation (shown in grey). Therefore, effect (iv) does not appear to be significant, at least when a relatively refined DB mesh is employed.

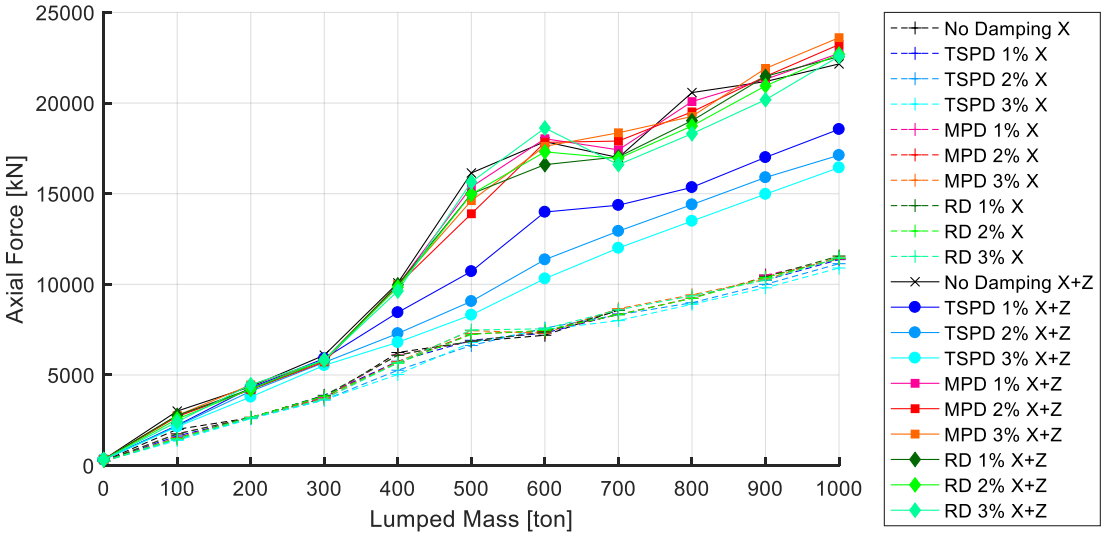

Figure 4. Maximum compressive forces for the CHHC ground motion, using one FB element.

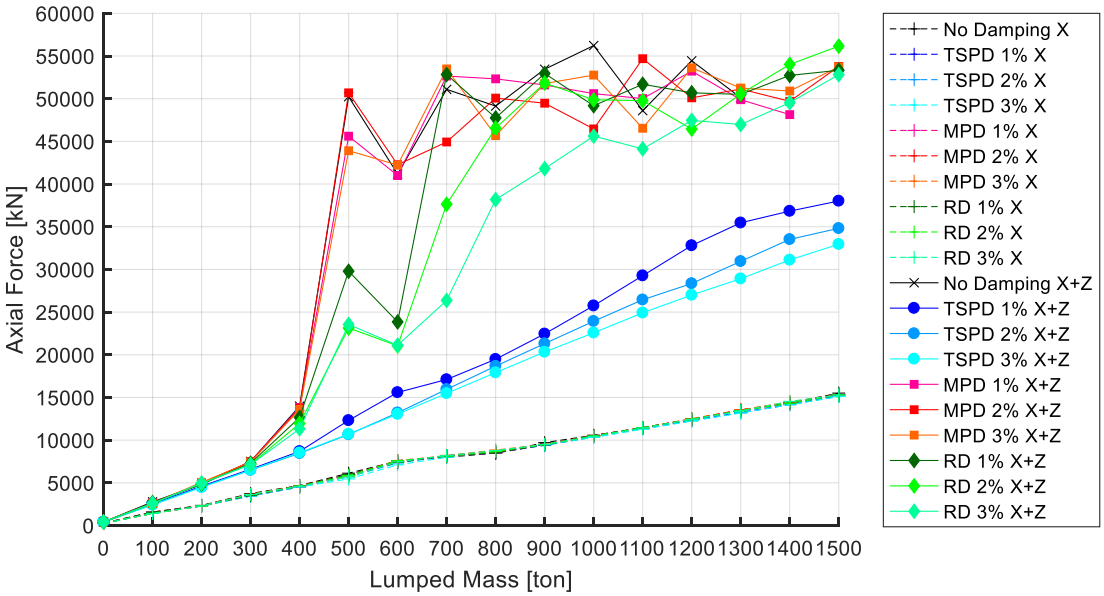

Figure 5. Maximum compressive forces for the (scaled) PRPC ground motion, using one FB element.

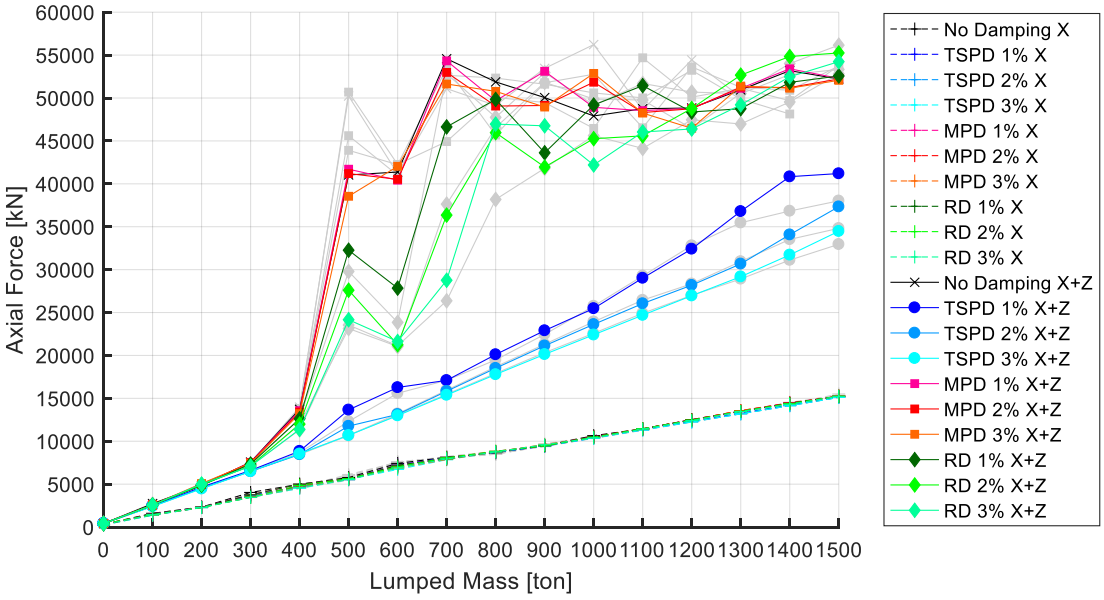

Figure 6. Maximum compressive forces for the (scaled) PRPC ground motion, using a four-element DB mesh (in grey the results with one FB element, as depicted in Figure 5).

5.2.2 Maximum Tensile Forces

Figure 7 and Figure 8 below show the maximum tensile forces attained during the CHHC and scaled PRPC ground motions respectively, using four DB elements. It is again recalled that tension forces are plotted as negative values while compression forces as positive values. It can be observed that:

- Once again, the same three groups of curves show up. The influence of the vertical component of the ground motion (X+Z) is largely apparent.
- In some cases, very significant tensile forces were obtained, even larger in absolute value than the compressive axial forces from gravity loads.
- TSPD models fail to capture the expected maximum tensile force demands due to overdamping of the vertical vibration mode.
- Results with the DB mesh were more stable than with the FB formulation (in grey).

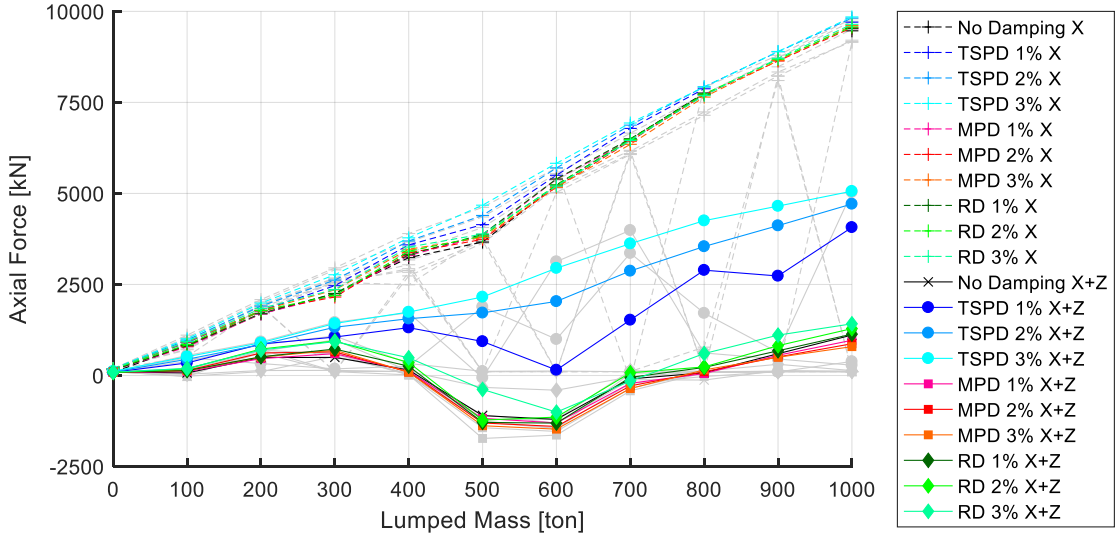

Figure 7. Maximum tensile forces for the CHHC ground motion, using a four-element DB mesh (in grey the results with one FB element).

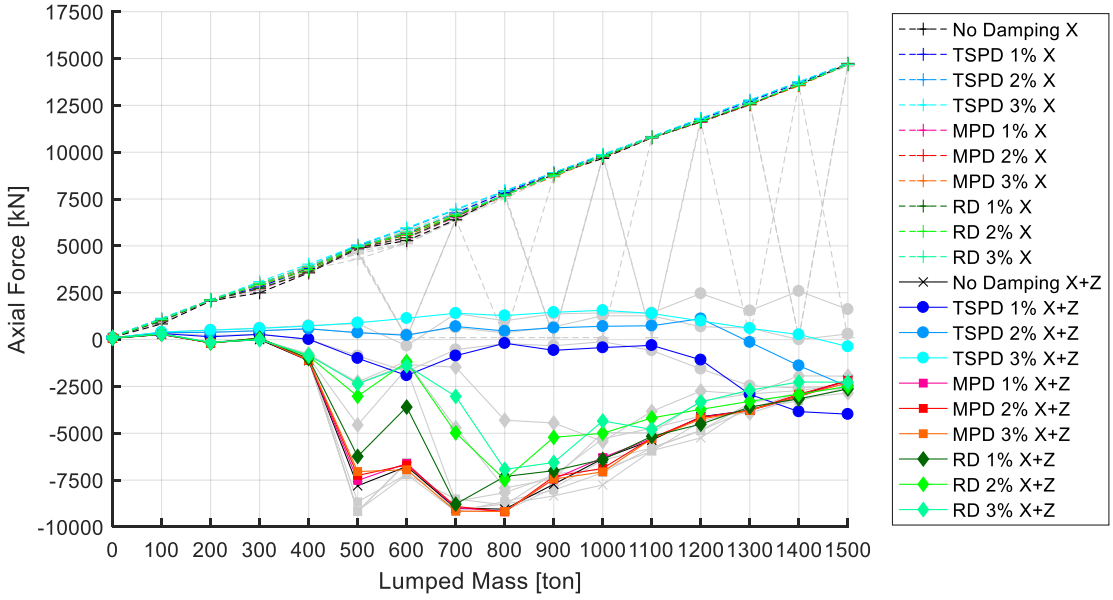

Figure 8. Maximum tensile forces for the (scaled) PRPC ground motion, using a four-element DB mesh (in grey the results with one FB element).

6. CONCLUSIONS

The present paper addresses the effect of the vertical component of ground motions on the structural response of RC structures. In particular, it focusses on how alternative common ways of modelling damping can influence the simulation of axial forces. A cantilevered bridge column with a top mass is used as an example. A range of prevalent vibration periods for horizontal and vertical components, associated to different values of the top mass (and therefore axial load ratio), was investigated. The impact of distinct beam finite element formulations was also analysed. The following main conclusions were obtained:

- The influence of the vertical ground motion component can be very significant. Maximum compressive forces can be increased several fold (increasing the potential for compression

failures), while non-negligible tensile forces, sometimes larger in absolute value than the compressive axial forces from gravity loads, can also show up (consequently reducing the shear strength).

- When only the horizontal ground motion component is applied, estimates of the axial forces are basically insensitive to different damping models and values, but the latter play a key role when the vertical component is also added to the simulation.
- Tangent stiffness-proportional damping, or Rayleigh damping as usually employed in practice (with damping ratios assigned to the modal frequencies that mostly contribute to the lateral response), are not suitable to model the effects of the vertical ground motion component. They artificially and significantly overdamp the vertical vibration mode, arguably underestimating the maximum tensile and compressive forces. Mass proportional-damping, or Rayleigh damping with damping ratios associated to lateral and vertical modes, appear to be more reasonable modelling choices to simulate the effect of the vertical component.
- Even though very small damping values were considered in this study (between 1% and 3%), such minor variations can have a significant influence on the results, namely for tangent stiffness-proportional damping. Together with the point above, this conclusion reinforces the need to carefully employ this damping model.
- Results with FB beam formulations and DB approaches are consistent, provided that a refined mesh is used for the latter.

6. REFERENCES

Ambraseys NN, Simpson AK (1996). Prediction of Vertical Response Spectra in Europe. *Earthquake Engineering & Structural Dynamics*, 25(4): 401–12.

Dionisio B (1994). Viscous Damping in Inelastic Structural Response. *Journal of Structural Engineering*, 120(4): 1240–54.

Bozorgnia Y, Campbell KW (2004). The Vertical-to-Horizontal Response Spectral Ratio and Tentative Procedures for Developing Simplified V/H and Vertical Design Spectra. *Journal of Earthquake Engineering*, 8(2): 175–207.

Bozorgnia Y, Niazi M (1993). Distance Scaling of Vertical and Horizontal Response Spectra of the Loma Prieta Earthquake. *Earthquake Engineering & Structural Dynamics*, 22(8): 695–707.

Bozorgnia Y, Niazi M, Campbell KW (1995). Characteristics of Free-Field Vertical Ground Motion during the Northridge Earthquake. *Earthquake Spectra*, 11(4): 515–25.

Bray JD, Rodriguez-Marek A (2004). Characterization of Forward-Directivity Ground Motions in the near-Fault Region. *Soil Dynamics & Earthquake Engineering*, 24(11): 815–28.

Calabrese A, Almeida JP, Pinho R (2010). Numerical Issues in Distributed Inelasticity Modeling of RC Frame Elements for Seismic Analysis. *Journal of Earthquake Engineering*, 14(sup1): 38–68.

Charney FA (2008). Unintended Consequences of Modeling Damping in Structures. *Journal of Structural Engineering*, 134(4): 581–92.

Chopra AK, Mckenna F (2017). Modeling Viscous Damping in Nonlinear Response History Analysis of Buildings. *16th World Conference on Earthquake Engineering*, 1–10, Santiago, Chile.

Chopra AK., McKenna F (2016). Modeling Viscous Damping in Nonlinear Response History Analysis of Buildings for Earthquake Excitation. *Earthquake Engineering & Structural Dynamics*, 45(2): 193–211.

Collier CJ, Elnashai AS (2001). A Procedure for Combining Vertical and Horizontal Seismic Action Effects. *Journal of Earthquake Engineering*, 5(4): 521–39.

Cooper M, Carter R, Fenwick R (2012). Final Report, Volume 4: Earthquake Prone Buildings. Report by Canterbury Earthquakes Royal Commission, Wellington, New Zealand.

Correia AA, Almeida JP, Pinho R (2013). Seismic Energy Dissipation in Inelastic Frames: Understanding State-of-the-Practice Damping Models. *Structural Engineering International*, 23(2): 148–58.

Filippou FC, Popov EP, Bertero VV (1983). Effect of Bond Deterioration on Hysteretic Behavior of Reinforced Concrete Joints. Earthquake Engineering Research Center, University of California, Berkeley, California.

GeoNet (2016). GeoNet - the Official Source of Geological Hazard Information for New Zealand, Available: https:/www.geonet.org.nz/quakes/felt.

Grant DN, Blandon C, Priestley MJN (2005). Modelling Inelastic Response in Direct Displacement-Based Design. IUSS Press, Pavia, Italy.

Hall JF (2006). Problems Encountered from the Use (or Misuse) of Rayleigh Damping. *Earthquake Engineering & Structural Dynamics*, 35(5): 525–45.

Hilber HM, Hughes TJR, Taylor RL (1977). Improved Numerical Dissipation for Time Integration Algorithms in Structural Dynamics. *Earthquake Engineering & Structural Dynamics*, 5(3): 283–92.

Jacobsen LS (1930). Steady Forced Vibrations as Influenced by Damping. *ASME Transactions*, 52(1): 169–181.

Jehel P, Léger P, Ibrahimbegovic A (2014). Initial versus Tangent Stiffness-Based Rayleigh Damping in Inelastic Time History Seismic Analyses. *Earthquake Engineering & Structural Dynamics*, 43(3): 467–84.

Kim SJ, Holub CJ, Elnashai AS (2011a). Analytical Assessment of the Effect of Vertical Earthquake Motion on RC Bridge Piers. *Journal of Structural Engineering*, 137(2): 252–60.

Kim SJ, Holub CJ, Elnashai AS (2011b). Experimental Investigation of the Behavior of RC Bridge Piers Subjected to Horizontal and Vertical Earthquake Motion. *Engineering Structures*, 33(7): 2221–35.

Lanzi A, Luco JE (2017). Influence of Viscous Damping Models on Inelastic Seismic Response of Fixed and Base-Isolated Structures. *16th World Conference on Earthquake Engineering*, 1–12, Santiago, Chile.

Lee H, Mosalam KM (2014). Seismic Evaluation of the Shear Behavior in Reinforced Concrete Bridge Columns Including Effect of Vertical Accelerations. *Earthquake Engineering & Structural Dynamics*, 43(3): 317–37.

Mander JB, Priestley MJN, Park R (1988). Theoretical Stress-Strain Model for Confined Concrete. *Journal of Structural Engineering*, 114(8): 1804–26.

Menegotto M., Pinto PE (1973). Method of Analysis for Cyclically Loaded RC Plane Frames Including Changes in Geometry and Non-Elastic Behaviour of Elements under Combined Normal Force and Bending. In *IABSE Symposium on Resistance and Ultimate Deformability of Structures Acted on by Well Defined Repeated Loads - Final Report*.

Newmark NM, Blume JA, Kapur KK (1973). Seismic Design Spectra for Nuclear Power Plants. *Journal of the Power Division*, 99(P02): 287–303.

Newmark NM, Hall WJ (1982). Earthquake Spectra and Design. *EERI Monographs*.

OpenSees (2013). Open System for Earthquake Engineering Simulation - Version 2.4.3.

Papazoglou AJ, Elnashai AS (1996). Analytical and Field Evidence of the Damaging Effect of Vertical Earthquake Ground Motion. *Earthquake Engineering & Structural Dynamics*, 25(10): 1109–37.

Priestley MJN, Calvi GN, Kowalsky MJ (2007). Displacement-Based Seismic Design of Structures, IUSS Press.

Priestley MJN, Grant DN (2005). Viscous Damping in Seismic Design and Analysis. *Journal of Earthquake Engineering*, 9(Special Issue 2): 229–55.

Puthanpurayil AM, Lavan O, Carr AJ, Dhakal RP (2016). Elemental Damping Formulation: An Alternative Modelling of Inherent Damping in Nonlinear Dynamic Analysis. *Bulletin of Earthquake Engineering*, 14(8): 2405–2434.

Sarno LDi, Elnashai AS, Manfredi G (2011). Assessment of RC Columns Subjected to Horizontal and Vertical Ground Motions Recorded during the 2009 L'Aquila (Italy) Earthquake. *Engineering Structures*, 33(5): 1514–35.

SeismoSoft (2016). SeismoStruct 2016 - A Computer Program for Static and Dynamic Nonlinear Analysis of Framed Structures, Available from http://www.seismosoft.com.

Terzic V, Schoettler MJ, Restrepo JI, Mahin S (2015). Concrete Column Blind Prediction Contest 2010: Outcomes and Observations. PEER Report No. 2015/01, Pacific Earthquake Engineering Research Center, University of California, Berkeley, USA.